HHS Public Access

Author manuscript

Nanomedicine. Author manuscript; available in PMC 2021 February 01.

Published in final edited form as:

Nanomedicine. 2020 August ; 28: 102213. doi:10.1016/j.nano.2020.102213.

Real time ultrasound molecular imaging of prostate cancer with PSMA-targeted nanobubbles

Reshani H. Perera, PhD[a], **Al de Leon, PhD**[a], **Xinning Wang, PhD**[b], **Yu Wang, MD, PhD**[a], **Gopal Ramamurthy, PhD**[a], **Pubudu Peiris, PhD**[b], **Eric Abenojar, PhD**[a], **James P. Basilion, PhD**[a,b], **Agata A. Exner, PhD**[a,b,*]

[a]Department of Radiology, Case Western Reserve University, Cleveland, OH, USA

[b]Department of Biomedical Engineering, Case Western Reserve University, Cleveland, OH, USA

Abstract

Contrast-enhanced ultrasound with microbubbles has shown promise in detection of prostate cancer (PCa), but sensitivity and specificity remain challenging. Targeted nanoscale-contrast agents with improved capability to accumulate in tumors may result in prolonged signal enhancement and improved detection of PCa with ultrasound. Here we report nanobubbles (NB) that specifically targets prostate specific membrane antigen (PSMA) overexpressed in PCa. The PSMA-targeted-NB (PSMA-NB) were utilized to simultaneously image dual-flank PCa (PSMA-positive PC3pip and PSMA-negative PC3flu) to examine whether the biomarker can be successfully detected and imaged in a mouse model. Results demonstrate that active targeting rapidly and selectively enhances tumor accumulation and tumor retention. Importantly, these processes could be visualized and quantified, in real-time, with clinical ultrasound. Such demonstration of the immense yet underutilized potential of ultrasound in the molecular imaging area can open the door to future opportunities for improving sensitivity and specificity of cancer detection using parametric NB-enhanced ultrasound imaging.

Keywords

Prostate cancer; Prostate specific membrane antigen; Ultrasound contrast agents; Nanobubbles; Ultrasound molecular imaging

Introduction

Despite significant efforts, prostate cancer (PCa) is still the second most common leading cause of cancer-related deaths worldwide, with 180,000 new cases diagnosed in the USA in 2018.[1,2] Accurate diagnosis of PCa is a crucial step necessary for informing the clinical management of the disease, yet conventional options leave much space for improvement. Currently, men with an abnormal digital rectal exam and/or increased levels of prostate

*Corresponding author at: Department of Radiology, Case Western Reserve University, Cleveland, OH, 44106, USA. agata.exner@case.edu (A.A. Exner).

Appendix A. Supplementary data

Supplementary data to this article can be found online at https://doi.org/10.1016/j.nano.2020.102213.

serum antigen (PSA) are considered at high risk for cancer and are referred for a prostate biopsy to assess if PCa is present. The standard PCa biopsy procedure uses transrectal ultrasound (US)-guidance to determine the prostate gland orientation, but the delineation of tumors within the prostate using US is unclear. Accordingly, biopsies are performed in a systematic manner by selecting 6–12 or more area from the peripheral zone of the prostate. These cores represent only 1% of prostate tissue and are a gross under sampling of prostate gland tissue, and biopsies performed using this conventional procedure result in significant false negatives of up to 50%.[3–5] Concern over the lack of pathological data in the face of other positive clinical risk factors results in almost 50% of patients undergoing second, if not third and fourth, prostate biopsies leading to increased costs and risk associated with unnecessary procedures. If the already-on board US technology can be used to more reliably identify the location of PCa within the prostate gland, these outcomes stand to be significantly improved.

Contrast-enhanced ultrasound has been investigated as one option for improved PCa detection.[6,7] In order to increase the PCa detection rate while limiting the number of biopsy procedures, significant effort has been focused on formulation of lipid and/or protein-stabilized gas-filled ultrasound contrast agents (UCAs) to improve the US imaging capability of cancer within the prostate.[8–10] Most of these efforts have utilized micron-sized UCAs or microbubbles (MBs),[9,11,12] which are already clinically utilized for other applications, but these have lacked specificity and sensitivity over conventional methods. One option to improve these parameters is molecular targeting of microbubbles to vascular-biomarkers. One example of this approach currently in clinical trials is BR55 (Bracco, Geneva, Switzerland),[13–15] which is targeted to vascular endothelial growth factor receptor-2 (VEGFR2). BR55 was examined recently in a clinical study for its ability to detect PCa[16]. The reported detection of malignant lesions with BR55 was 68%.[16] Two factors may confound the use of MBs for this application. The first is their large footprint, which confines MBs to the blood stream, and makes consistent targeting and retention at vascular markers challenging. It also makes most biomarkers for PCa and other cancer inaccessible, since most lie beyond the vasculature in the tumor parenchyma. Second, MBs have a short lifespan (typically <10 min) in the circulation, making their utility limited during targeting and the entire biopsy procedure.

These unmet needs have led to increased interest in nano-sized UCAs that can penetrate the tumor parenchyma, bind to cancers, and exhibit nonlinear contrast behavior similar to MBs.[17–22] Our group has recently developeda stable nanobubble (NB) UCA that contains perfluoropropane inside a propylene glycol and glycerol-enhanced lipid shell. These NBs demonstrate unique physicochemical properties and an extended life span *in vivo*[23,24]. Due to their reduced hydrodynamic diameter, NBs should have the ability to pass though hyper-permeable vasculature in tumors.[25–27] Furthermore, active targeting to a biomarker overexpressed on PCa should enhance the retention of administered NBs at the tumor site, thus facilitating enhanced molecular contrast imaging in the tumor. A well-known biomarker for PCa is the prostate specific membrane antigen (PSMA).[28–30] PSMA is a type II integral membrane protein that is expressed at lower levels in the healthy prostate and other organs such as the kidney, liver, and brain, but significantly at higher levels in PCa.[31,32] The level of PSMA has a positive correlation with the pathological phase of the tumor stage[33–35] and is

also considered to be the most important protein target in diagnostic specific immunolocalization imaging and immune-directed therapy.[31,33,36] Many ligands specific to PSMA are available, including monoclonal and engineered antibodies, small sized molecules, nanobodies, and aptamers.[9,10]

In the current study, we demonstrate the use of standard nonlinear contrast-enhanced US for real-time molecular imaging of PCa by targeting stable NBs to PSMA *via* the PSMA-1 ligand, which has been previously validated as a robust marker for PCa[37,38] (Figure 1, A). Our data demonstrate significant, sustained differences between the kinetics of PSMA-NB, NB and MB in PCa models. Specifically, the PSMA-NBs were rapidly taken up by the PSMA-expressing tumors and were selectively retained within the tumor parenchyma, significantly extending duration the signal available for US visualization compared to untargeted NBs and the commercially available MB, Lumason®. No differences were seen in the PSMA-negative tumors or kidneys between NBs and PSMA-NBs, suggesting that the observed retention is due to specific molecular targeting to PSMA in the tumor itself. Notably, since clinical US was consistently capable of distinguishing these kinetic differences in small tumors, the work lays the foundation for future work utilizing the technique in real-time US biopsy guidance.

Methods

Preparation and characterization of contrast agents

The preparation and characterization of base ultrastable-NBs has been reported elsewhere.[23,24,39] Details can be found in Supplementary Materials.

In vitro US stability of PSMA-NB in PBS and in blood-plasma

Blood was collected from a euthanized mouse by cardiac puncture and centrifuged to obtain the blood plasma. PSMA-NB solution was diluted 1:100 with PBS or blood plasma (1:10 diluted with PBS) and was placed in a tissue-mimicking agarose phantom as described previously.[24] Nonlinear ultrasound imaging was carried out using the AplioXG SSA-790A clinical ultrasound imaging system (Toshiba Medical-Imaging Systems, Otawara-Shi, Japan) with a 12 MHz center frequency linear array transducer (PLT-1204BT). Images were acquired in contrast harmonic imaging (CHI) mode with parameters set as: 65 dB dynamic range, 70 dB gain, and 0.2 frame-rate for 30 min. Optical-images were taken at 100X with OMAX-microscope (Model: M837ZL-C180U3).

Cell culture

Retrovirally-transformed PSMA-positive PC3pip cells and transfection-control PC3flu cells were originally obtained from Dr. Michel Sadelain (Memorial-Sloan Kettering Cancer Center, New York, NY). The two cell lines were checked and authenticated by western blot. Cells were grown at 37 °C and 5% CO_2 and maintained in complete RPMI1640 medium (Invitrogen Life Technology, Grand Island, NY).

Cellular uptake studies

PC3pip and PC3flu cells were plated on coverslips at about 70% confluence. Rhodamine-labeled-NBs were prepared by mixing DSPE-Rhodamine (50 μL) into the lipid solution. Twenty-four hours later, cells were incubated with Rhodamine-NBs for 1 h. After incubation, cells were washed (3X) with PBS, fixed with 4% paraformaldehyde, counterstained with 2-(4-amidinophenyl)-6-indolecarbamidine dihydrochloride (DAPI), mounted and observed under Leica (DM4000B) fluorescence-microscopy (Leica Microsystem Inc., Buffalo Grove, IL). The fluorescent intensity was then quantified by Image J. For the cell competition experiment, PC3pip cells (5×10^5) in 100 μL media were incubated with 100 μL of 1:30 diluted-NB for 1 h at 37 °C in Eppendorf Tubes, then 100 μL of 50 nM PSMA-Cys-Cy5.5 in RPMI was added and incubated for 1 h at 37 °C. Then wash 3× with 500 μL cold-PBS, resuspended in 100 μL-PBS and transferred to 96-well black plate. The fluorescence was measured on Tecan plate reader with Ex = 684 nm/Em = 710 nm.

Animal model

Mice were handled according to a protocol approved by the Institutional Animal Care and Use Committee (IACUC) at Case Western Reserve University and were in accordance with all applicable protocols and guidelines in regards to animal use. Male athymic nude mice (4–6 weeks old) were anesthetized with inhalation of 3% isoflurane with 1 L/min oxygen and were implanted subcutaneously with 1×10^6 of PSMA-negative PC3flu and PSMA-positive PC3pip cells in 100 μL matrigel. Animals were observed every other day until tumors reached at about 8–10 mm in diameter.

Pharmacokinetic study

Two weeks after tumor inoculation, the animals were used in the study (n = 7). The US probe (PLT-1204BT, AplioXG SSA-790A, Toshiba Medical-Imaging Systems, Otawara-Shi, Japan) was placed to visualize the ultrasound images of the PC3pip and PC3flu tumors and the kidney in the same field of view. Either undiluted Plain NB or PSMA-NB (200 μl) were administrated *via* tail-vein. After injection, the change of tissue contrast was measured using contrast harmonic imaging (CHI, frequency 12.0 MHz; MI, 0.1; dynamic-range, 65 dB; gain, 70 dB; imaging frame rate, 0.2 frames/s) for 30 min. The remaining NBs were burst by repeated flash replenish (high energy pulses). Thirty minutes later (1 h after first injection, the contrast was reached to baseline level) the same mouse received PSMA-NB or plain-NB respectively (n = 7). Lumason® (sulfur hexafluoride lipid-type-A microspheres, Bracco Diagnostics Inc.) were tested *in vivo* (n = 3). Lumason was prepared according to the protocol provided by the manufacturer. The raw data were processed with software provided by the scanner manufacturer. The kidney, and tumor areas were delineated by drawing regions of interest (ROIs) and the signal intensity in each ROI as a function of time (time-intensity curve-TIC) was calculated. The data were exported to Microsoft Excel, the baseline was subtracted from TIC, and the calculated peak value of TIC was used to normalize the data to obtain the decay of signal. Origin (OriginLab, Northampton, MA)-was used to calculate the area under the peak (AUC) and other TIC parameters.

Histological analysis

Animals were divided into 3-groups: Cy5.5-PSMA-NB (n = 3), Cy5.5-NB (n = 3), and no-contrast-control. Cy5.5 labeled NBs were prepared by mixing DSPE-PEG-Cy5.5 (100 μl) into the lipid solution. Mice received either 200 μl of undiluted UCAs or PBS *via* tail-vein. Twenty-five minutes after injection, animals were scanned using US to detect the signal and then PBS perfusion was performed with 50 ml PBS through left-ventricle. Then, tumors were scanned again to perceive the US signal that generate from intact-NB. Tumors and the kidney were harvested, fixed in paraformaldehyde and embedded in optimal-cutting-temperature compound (OCT Sakura Finetek USA Inc., Torrance, CA). The tissues were cut into 8 μm slices and washed (3x) with PBS and incubate with protein blocking solution that contain 0.5% TritonX-100 (Fisher Scientific, Hampton, NH) and incubated in 1:250 diluted primary-antibody CD31(PECAM-1) Monoclonal Antibody Fisher Scientific, Hampton, NH) for 24 h at 4 °C. After washed with PBS, incubated with Alexa-568 tagged secondary-antibody (Fisher Scientific, Hampton, NH) for 1 h and stained with DAPI (Vecor Laboratories, Burlingame, CA). The fluorescence images were obtained and analyzed (by interactive function of segmentation and threshold) using Axio Vision V 4.8.1.0, Carl Zeiss software (Thornwood, NY). For PSMA-immunohistochemistry, tissues were washed 3× with PBS and incubated with blocking solution followed by 1:150 diluted PSMA primary-antibody (Thermo Fisher Scientific, Waltham, MA) for 24 h at 4 °C and followed the above steps as for CD31 staining.

Statistical analysis

Graphs and statistical analyses were generated using Microsoft Excel and Origin. Unpaired Student's *t*-test (two-tailed) was used to compare two groups. Data are presented as a mean ± STD (standard-deviation). The experiments were repeated at least three times, unless stated otherwise.

Results

Validation and characterization of PSMA targeted NB

PSMA-Cys was conjugated to DSPE-PEG2K lipids through reaction of –SH group in PSMA-Cys with DSPE-PEG2K-maleimide. HPLC and MALDI-TOF-MS results confirmed the conjugation of PSMA-1 to the DSPE-PEG2K. The preparation and characterization of base ultrastable-NBs has been reported elsewhere.[23,24,39] The NB hydrodynamic-diameter and concentration were characterized using resonant mass measurement (RMM) capable of detecting both buoyant (bubbles) and non-buoyant particles (liposomes, micelles, lipid debris, *etc.*). The RMM technology operates by measuring the change in the frequency of oscillation of particles that flow through an oscillating cantilever.[23,40–42] The size and the concentration of PSMA-NB were 266–288 nm and $3.9 \times 10^{11} \pm 2.82 \times 10^{10}$ NBs/ml, respectively. The mean size and the concentration did not change significantly after DSPE-PSMA was incorporated into the NBs (Figure 1, B and Figure 1, C). Apart from gas filled bubbles, we also detected non-buoyant particles in both bubble solutions, which are invisible under US, but may contribute to the bubble overall stability[43] (Figure 1, B). The slightly negative values of zeta potential crucial to the stability of both targeted and untargeted NB (Figure 1, C) were also confirmed using DLS measurement. The rate of decay of US signal

in vitro stability was assessed by placing PSMA-NB solution in PBS in a narrow channel in a hydrogel phantom[39] as previously described. The channel ensures that all bubbles are exposed to the acoustic field for the duration of the experiment. Upon constant insonation at 0.2 fps, PSMA-NB displayed minimal signal decay in both PBS and blood plasma for over a 30 min time period (Figure S2). The calculated *in vitro* half-life of PSMA-NB in diluted blood plasma was ~3 h. PSMA-NB also did not demonstrate any perceivable aggregation in the blood plasma within the time tested (Figure S2, B).

In vitro cellular uptake studies

To optimize the amount of PSMA-1 ligand on the surface of NBs, bubbles with different amounts of PSMA-1 ligand were prepared, and labeled with Rhodamine B. The highest fluorescence was found in NBs labeled with reactions that contained 25 μg (35×10^3 PSMA-molecules/NB) of PSMA-1, followed by NBs with 50 μg (70×10^3 PSMA-molecules/NB) of PSMA-1, then decreased significantly in NBs with 100 μg (14×10^4 PSMA-molecules/NB) of PSMA-1 (Figure S3, A and B). Our results concurred with other reports that best targeting was observed in nanoparticles with intermediate number of ligands per nanoparticle.[44] After the optimal ligand density was established, we then compared the cellular uptake of Rhodamine-PSMA-NB in PSMA-positive PC3pip cells and PSMA-negative PC3flu cells as shown in Figure 2, A. When cells were exposed to Rhodamine-NB, similar fluorescence intensity was observed in PC3pip and PC3flu cells. When PC3flu cells were exposed to Rhodamine-PSMA-NB, the fluorescent intensity was not significantly different compared to cells exposed to Rhodamine-NB (Figure 2, B). In contrast, the signal increased dramatically in PC3pip cells (~10 fold increased), which express PSMA, when treated with Rhodamine-PSMA-NB, indicating that PSMA-NBs selectively bind to PSMA-expressing cells. Figure 2, C demonstrated a significant reduction of fluorescence intensity of PSMA-Cy5.5 in PC3pip cells in the presence of PSMA-NB, which confirm the PSMA-NB bound to the PC3pip cells. There was no significant difference between PSMA-Cy5.5 with and without PSMA-NB in PC3flu cells.

In vivo ultrasound imaging

In vivo experiments examining the kinetics of targeted PSMA-NB and NB were performed using clinical nonlinear contrast enhanced ultrasound, and the average results from 7 mice are reported (Figure 3). Five quantitative parameters related to perfusion and bubble dispersion were extracted from the acquired time-intensity-curves (TIC). These include peak intensity, time to peak, the duration of contrast enhancement, and area under the curve. The parameters were compared between PSMA-NB and NB in the PC3pip and PC3flu tumors. Additional comparison was made with the commercially available micro-bubble, Lumason®.

Both PC3pip and PC3flu tumors and kidneys were localized in the same field of view (FOV) using ultrasound B-mode imaging. Before injection, tumors and kidneys were not visible under ultrasound in the nonlinear contrast harmonic imaging (CHI) mode (Figure 3, A). A total of 200 μl of undiluted NB (~8×10^{10} PSMA-NB or NB) were injected through the tail vein, and continuous contrast mode US was performed to visualize the bubble dynamic in the tumors and the kidney. Rapid enhancement of the contrast was observed first in the

kidneys followed by both tumors approximately 30 sec to 2 min post-injection. The time to peak for PSMA-NB in the PC3pip tumor was slightly longer but it is not significantly different compared to that of PSMA-NB in PC3flu, (Figure S4, A; 3.97 ± 1.20 min compared to 2.75 ± 1.31 min, $P = 0.09$). Furthermore, there was no significant difference between the time to peak for NB in either PC3pip or PC3flu tumor ($P = 0.21$). The average peak intensity was measured to be 15.64 ± 0.42 dB for PSMA-NB and NB in the both tumors and it is not significantly different in each case (Figure S4, B). The NB accumulation was compared and validated using clinically available MB-Lumason®. The peak intensities obtained for PSMA-NB (15.96 ± 1.83 dB) and NB (15.60 ± 2.53 dB) were significantly different from the one observed with the Lumason® (7.38 ± 0.33 dB, $P < 0.001$). Also, the duration of signal enhancement with Lumason® was limited to <5 min indicating low stability and low circulation time of Lumason® MB in the blood stream.

Table 1 shows the quantitative parameters obtained from the time intensity curves, including peak enhancement, time to peak, area under the curve (AUC), and 25% of the maximum peak. Importantly, the AUC was calculated for wash in (WiAUC) and wash out (WoAUC) phases separately, since the main differences in bubble dynamics were expected during the washout phase. The total AUC is shown in Figure S4, C. The WiAUC for all cases were consistent, however, the WoAUC of PSMA-NB in PC3pip tumor showed a significant, 2-fold increase, compared to all other groups (Figure S4, D; $P < 0.001$). Since the TIC are similar in all cases at the early time points, but deviate at the later time points, the half peak maximum or the half time of peak intensity ($t_{50\%}$) was also similar between groups (data not shown). However, the time to reach 25% of the maximum peak intensity ($t_{75\%}$) for PSMA-NB in PC3pip tumor was 2-fold longer than all other groups ($P < 0.01$) (Table 1). These results indicated prolonged retention of targeted NB in PSMA-expressing tumors.

To further clarify the effect that active nanobubble targeting had on tumor accumulation, the signal from PSMA-NB was normalized to the signal from NB in both PC3pip and PC3flu tumors at selected time points. This was enabled by the fact that each mouse in the cohort received a randomized injection of both targeted and untargeted NBs. Thus, we can compare the effect of targeting, and of target expression in tissue, in addition to any unrelated confounding effects that may result from surface functionalization of the bubbles. Figure 4, A shows a significantly higher ratio (>2) at t = 15 min post-injection of bubbles in PC3pip tumor compared to the PC3flu tumor and was significantly different at each time point. The high ratio persisted, and in fact continued to increase, for up to 30 min. To minimize the effect of the variability in tumors between animal to animal, the signal from each bubble in both tumors was also normalized to the kidney signal of the same animal at each time points. The kidney represents “normal tissue” where no extravascular accumulation of the NBs would be expected. Figure 4, B again revealed consistently increasing signal only in the PSMA-NB in the PC3pip tumors. These bubbles showed >2-fold high normalized signal compared to that of all the other groups at the study endpoint.

No significant differences were noted between PSMA-NB and NB groups for the time to peak, peak max, WiAUC in kidneys. Although the AUC in kidney with PSMA-NB injection was higher compared to the NB group, there is no significant difference between the two

types of NBs (Figure S4, C). Moreover, in the kidneys there was no significant difference in $t_{50\%}$ or $t_{75\%}$ values between PSMA-NB and NB (data not shown).

Histology

To further validate that PSMA-targeted NB can extravasate into the tumor matrix, the bubbles were tagged with a fluorescent dye; Cy5.5, and injected *via* tail vein. Twenty-five minutes post-injection, the anesthetized animal was euthanized using cardiac perfusion with saline to remove all blood and concurrently all circulating bubbles. The tumors and kidneys were harvested for histological analysis. In animals harboring the PC3pip tumors, the Cy5.5-PSMA-NB signal can be seen deep in the tissue, distally from the microvasculature, providing strong evidence that the targeted NBs extravasate from the vasculature and enter the tumor interstitial space (Figure 5, A). The Cy5.5-PSMA-NB signal in PC3pip tumor was significantly higher (5.4-fold) compared to retained signal in tumors that did not express PSMA, PC3flu tumor ($P < 0.001$) (Figure 5, B). Likewise, non-targeted Cy5.5-NB had low accumulation in both PC3pip and PC3flu tumors, which was comparable to targeted NB levels in the PC3flu tumors after perfusion. We noted no significant histological differences of vasculature between both types of tumors when sections were stained with anti-CD-31 (Figure 5, B). Quantification of the Cy5.5 labeled bubbles revealed that the targeted bubbles showed 5-fold more accumulation and localization with the CD31 stained vasculature in the PC3pip compared to PC3flu tumors (Figure 5, D). The overexpression of the PSMA in the PC3pip cells was confirmed by immunohistochemistry results (Figure 5, C, E; 63.66 ± 1.51 *vs* 1.83 ± 0.15).

Discussion

PCa biopsies frequently provide false negative results. Consequently, there is a critical need for improved tools for PCa detection that can be used to better inform biopsy procedures. A wide range of imaging approaches is being examined to fill this unmet need, with MRI-guided biopsies and MRI preplanning showing the most promise.[45–50] Multiparametric MRI (mpMRI) and MRI-guided in gantry biopsies have been used in the clinic, and some sites have shown that the rate of PCa detection with these procedures is improved compared to transrectal US-guided biopsies.[46–50] However, MRI-based exams and procedures still present a number of challenges for broad adoption: they are not widely available, they are not portable and have a confined working space, and they require additional expertise outside of urology (*e.g.* radiology). The procedures can also be quite expensive and add significant time and cost to the diagnostic workflow. Finally, the negative predictive value (the ability to confidently state that a patient is malignancy-free), while hugely beneficial, has not been shown to be effective at this point with MRI.[51,52]

A large body of work has instead focused on use of contrast-enhanced US that are capable of molecular level imaging for this application. However, due to the rapid dissipation of encapsulated gas that causes a rapid signal decay, MB have a short *in vivo* half-life, which is not subtle enough to delineate pathological tissues from surrounding normal tissues for US-guided biopsies. Currently, the most promising MB tool is BR55, which targets VEGFR2,[14,15,53] as discussed above, also has comparatively low specificity and sensitivity.

While MBs are useful for visualizing vascular targets, they are restricted to the blood pool. In contrast, nano-sized particles may be able to penetrate leaky tumor vasculature to reach tissue targets located outside of vessels. In the current study, in order to achieve specific US molecular imaging, the NBs were targeted to PSMA, which is expressed in high level in both androgen-dependent and independent PCa, and a common target for PCa US-imaging.[9,10] Consequently, PSMA-1 tagged NBs open an avenue for specific imaging at a molecular level in the tumor environment.

Bubble diameter and concentration obtained using resonant mass measurement indicated that both NB and the PSMA-NB are in nanoscale (<300 nm) range and have a concentration several orders of magnitude higher than commercial MB agents. The small size and high shell deformability facilitated by inclusion of the edge activator, propylene glycol[54] may enable NBs to pass through the neovasculature.[55,56] In addition, it should be pointed out that the C_3H_8 gas contained in the core of the nanobubble formulation is used in clinical FDA-approved formulations such as Definity® MB. This contrast material has been used for over 20 years and has not exhibited significant toxic side effects.[57] With a similar gas volume upon injection, it is expected that the toxicity of C_3F_8 nanobubbles would be comparable to Definity.

The *in vitro* cell uptake studies provided the optimum concentration of PSMA-1 that can be incorporated into the NBs to achieve peak uptake. The optimum ligand density obtained (35×10^3 ligands/NB) concurred with the reported values.[44] Cell uptake studies also demonstrated selectivity of binding of PSMA-NBs to the PSMA-positive-PC3pip tumor cells. In the *in vivo* acoustic evaluation, the nondestructive low mechanical index (MI = 0.1) was used to construct TIC and the parametric dynamic CEUS imaging was used to derive the contrast kinetics. Most importantly, this data demonstrates selective uptake of PSMA-NB in PSMA-positive PC3pip tumors compared to the PSMA-negative PC3flu tumors. In comparing the contribution of active targeting to this behavior it was crucial to also examine untargeted NB in the same tumors, thus mice received a randomized injection of these bubbles in the same exam, either before or after PSMA-NB administration. We observed that the time to peak and maximum peak enhancement were similar in both groups, signifying the similar dynamic of PSMA-NB and NB in the blood stream and also comparable morphology and vasculature in both PC3pip and PC3flu tumors. In stark contrast, the washout was slower with PSMA-NB in the PC3pip tumor compared to all other groups, as shown by persistent enhancement over 30 min, 2-fold higher WoAUC and $t_{75\%}$. Preferential accumulation of PSMA-NB in the PSMA expressing tumors was noticeable as early as 10 min after injection and increased over time. This is a considerable improvement over the relatively small and transient differences noted in prior studies of PSMA-targeted UCAs.[9,10] Furthermore, the extent of PSMA-NB binding to the target site may be somewhat limited by the co-injection of any free PSMA-1 ligand that was not incorporated into the NB formulation. In preliminary *in vitro* experiments using size exclusion chromatography to purify PSMA-NBs before use, total NB binding increased by 34% (data not shown). This technique will be used in future studies to further increase binding efficiency *in vivo.* Lumason® exhibited significant rapid enhancement in the kidney and relatively minor enhancement in tumors, and were cleared from the circulation rapidly without any significant binding. The data obtained for Lumason® was comparable to previously reported

data for Lumason® kinetics.[58] The high tumor to kidney signal ratio with PSMA-NB in PC3pip tumor also supports the conclusion that targeted NBs accumulate in PSMA-expressing tumors. However, to fully elucidate the fate of NB in the tumor tissue, a 3D imaging modality will be more informative compared to 2D imaging; these studies are currently ongoing.

Histological findings confirm the PSMA targeted NB can specifically recognize the tumors with PSMA expression. The percentage of PSMA-NB in PC3pip tumor is approximately 6-fold higher than that in PC3flu tumor. There bubbles were previously shown to also be intact and capable of generating acoustic activity, even following tumor perfusion.[59] The data also revealed that PSMA appears to be present in the tumor vasculature, which is a well-documented phenomenon for many tumors including some prostate cancers.[60] Concurrent with this we observed signal from PSMA-NB in the neovasculature in some PC3pip tumors even after the whole body perfusion of the animal (data not shown). Moreover, the histology data showed an increase of PSMA-NB accumulation in kidneys. While absolute levels were small, the PSMA-NB signal in the kidney was on average 6-fold higher compared to the NB signal (Figure S4, A and B). Notably, we observed positive signal from PSMA in kidney, yet approximately 30% lower compared to the PC3pip tumor (Figure S4, C). Despite this unexpected expression, the kidney normalized data in Figure 4, B shows increasing enhancement in the PC3pip tumors over 30 min, indicating the affinity, biding and retention of PSMA-NBs in tumors is considerable.

The prolonged-persistence of US signal of PSMA-NB in PCa provides exciting future opportunities to facilitate improved PCa detection with multiparametric contrast-enhanced ultrasound. The same principles can also make real-time PCa biopsies with US guidance a reality in the future. Additional studies are ongoing to also examine in detail extravasation of nanobubbles in tumors and quantify their acoustic activity following extravasation. Furthermore, in depth studies will elucidate the capability of PSMA-NB in delineating PCa using orthotropic PCa in mouse and larger animal models with the eventual goal of clinical translation into a rapid real-time biopsy guidance strategy.

Supplementary Material

Refer to Web version on PubMed Central for supplementary material.

Acknowledgements

This work was funded by the National Institutes of Health (R01EB025741) and the Office of the Assistant Secretary of Defense for Health Affairs, through the Prostate Cancer Research Program under Award No. W81XWH-16-1-037I and W81XWH-16-1-0372. We also acknowledge additional support from the Case Comprehensive Cancer Center P30CA043703 in the form of a pilot grant and National Foundation for Cancer Research (NFCR). We would like to thank Dr. C. Hernandez, Dr. A. Akhter, Dr. J. Lilly and Dr. B. Erokwu for their initial assistance with these studies. Also, we would like to acknowledge Pinunta Nittayacharn for assistance with purifying the nanobubble samples.

Funding Sources: This work was funded by the National Institutes of Health (R01EB025741) and the Office of the Assistant Secretary of Defense for Health Affairs, through the Prostate Cancer Research Program under Award No. W81XWH-16-1-0371 and W81XWH-16-1-0372. We also acknowledge additional support from the Case Comprehensive Cancer Center P30CA043703 in the form of a pilot grant and National Foundation for Cancer Research (NFCR). Views and opinions of, and endorsements by the author(s) do not reflect those of the National Institutes of Health or of the Department of Defense. The authors report no conflicts of interest to this work.

Abbreviations:

PCa	prostate cancer
NB	nanobubbles
PSMA	prostate specific membrane antigen
PSMA-NB	PSMA-targeted-NB
UCAs	ultrasound contrast agents
US	ultrasound
PSA	prostate serum antigen
VEGFR2	vascular endothelial growth factor receptor 2
CHI	contrast harmonic imaging
DBPC	1,2-dibehenoyl-snglycero-3-phosphocholine
DPPA	1,2 Dipalmitoyl-sn-Glycero-3-Phosphate
DPPE-1	2-dipalmitoyl-sn-glycero-3-phosphor ethanolamine
DSPE-mPEG 2000	1,2- distearoyl-snglycero-3-phosphoethanolamine-N-(ammonium salt)
C_3F_8	octafluoropropane
DSPE-PEG-MAL-1	2-distearoylsnglycero-3-phospho ethanolamine-N-[methoxy(polyethylene glycol)-2000-Maleimide
HPLC	high performance liquid chromatography
MALDI-TOF-MS	matrix-assisted laser desorption/ionization time-of-flight mass spectroscopy
DAPI	2-(4-amidinophenyl)-6-indolecarbamidine dihydrochloride
OCT	optimal-cutting-temperature compound
RMM	resonant mass measurement
TIC	time-intensity curves
AUC	area under the curve
WiAUC	wash-in area under the curve
WoAUC	wash out area under the curve

References

1. Negoita S, Feuer EJ, Mariotto A, Cronin KA, Petkov VI, Hussey SK, et al. Annual Report to the Nation on the Status of Cancer, Part II: recent changes in prostate cancer trends and disease characteristics. Cancer 2018;124(13):2801–14. [PubMed: 29786851]
2. Cronin KA, Lake AJ, Scott S, Sherman RL, Noone AM, Howlader N, et al. Annual Report to the Nation on the Status of Cancer, Part I: national cancer statistics. Cancer 2018;124(13):2785–800. [PubMed: 29786848]
3. Mottet N, Bellmunt J, Bolla M, Briers E, Cumberbatch MG, De Santis M, et al. EAU-ESTRO-SIOG Guidelines on Prostate Cancer. Part 1: screening, diagnosis, and local treatment with curative intent. Eur Urol 2017;71(4):618–29. [PubMed: 27568654]
4. Roethke M, Anastasiadis AG, Lichy M, Werner M, Wagner P, Kruck S, et al. MRI-guided prostate biopsy detects clinically significant cancer: analysis of a cohort of 100 patients after previous negative TRUS biopsy. World J Urol 2012;30(2):213–8. [PubMed: 21512807]
5. Pallwein L, Mitterberger M, Pelzer A, Bartsch G, Strasser H, Pinggera GM, et al. Ultrasound of prostate cancer: recent advances. Eur Radiol 2008;18(4):707–15. [PubMed: 17938936]
6. Smeenge M, Barentsz J, Cosgrove D, de la Rosette J, de Reijke T, Eggener S, et al. Role of transrectal ultrasonography (TRUS) in focal therapy of prostate cancer: report from a consensus panel. BJU Int 2012;110(7):942–8. [PubMed: 22462566]
7. Smeenge M, de la Rosette JJ, Wijkstra H. Current status of transrectal ultrasound techniques in prostate cancer. Curr Opin Urol 2012;22 (4):297–302. [PubMed: 22595778]
8. Sanna V, Pintus G, Bandiera P, Anedda R, Punzoni S, Sanna B, et al. Development of polymeric microbubbles targeted to prostate-specific membrane antigen as prototype of novel ultrasound contrast agents. Mol Pharm 2011;8(3):748–57. [PubMed: 21545176]
9. Wang L, Li L, Guo Y, Tong H, Fan X, Ding J, et al. Construction and in vitro/in vivo targeting of PSMA-targeted nanoscale microbubbles in prostate cancer. Prostate 2013;73(11):1147–58. [PubMed: 23532872]
10. Fan X, Wang L, Guo Y, Tu Z, Li L, Tong H, et al. Ultrasonic nanobubbles carrying anti-PSMA nanobody: construction and application in prostate cancer-targeted imaging. PLoS One 2015;10(6)e0127419. [PubMed: 26111008]
11. Zlitni A, Yin M, Janzen N, Chatterjee S, Lisok A, Gabrielson KL, et al. Development of prostate specific membrane antigen targeted ultrasound microbubbles using bioorthogonal chemistry. PLoS One 2017;12(5) e0176958. [PubMed: 28472168]
12. Hernot S, Unnikrishnan S, Du Z, Shevchenko T, Cosyns B, Broisat A, et al. Nanobody-coupled microbubbles as novel molecular tracer. J Control Release 2012;158(2):346–53. [PubMed: 22197777]
13. Willmann JK, Bonomo L, Carla Testa A, Rinaldi P, Rindi G, Valluru KS, et al. Ultrasound molecular imaging with BR55 in patients with breast and ovarian lesions: first-in-human results. J Clin Oncol 2017;35 (19):2133–40. [PubMed: 28291391]
14. Tardy I, Pochon S, Theraulaz M, Emmel P, Passantino L, Tranquart F, et al. Ultrasound molecular imaging of VEGFR2 in a rat prostate tumor model using BR55. Invest Radiol 2010;45(10):573–8. [PubMed: 20808233]
15. Pochon S, Tardy I, Bussat P, Bettinger T, Brochot J, von Wronski M, et al. BR55: a lipopeptide-based VEGFR2-targeted ultrasound contrast agent for molecular imaging of angiogenesis. Invest Radiol 2010;45 (2):89–95. [PubMed: 20027118]
16. Smeenge M, Tranquart F, Mannaerts CK, de Reijke TM, van de Vijver MJ, Laguna MP, et al. First-in-human ultrasound molecular imaging with a VEGFR2-specific ultrasound molecular contrast agent (BR55) in prostate cancer: a safety and feasibility pilot study. Invest Radiol 2017;52(7):419–27. [PubMed: 28257340]
17. de Leon A, Perera R, Nittayacharn P, Cooley M, Jung O, Exner AA. Ultrasound contrast agents and delivery systems in cancer detection and therapy. Adv Cancer Res 2018;139:57–84. [PubMed: 29941107]

18. Gao Y, Hernandez C, Yuan HX, Lilly J, Kota P, Zhou H, et al. Ultrasound molecular imaging of ovarian cancer with CA-125 targeted nanobubble contrast agents. Nanomedicine 2017;13(7):2159–68. [PubMed: 28603079]
19. Perera RH, Wu H, Peiris P, Hernandez C, Burke A, Zhang H, et al. Improving performance of nanoscale ultrasound contrast agents using N. N-diethylacrylamide stabilization Nanomedicine 2017;13(1):59–67. [PubMed: 27565686]
20. Perera RH, Hernandez C, Zhou H, Kota P, Burke A, Exner AA. Ultrasound imaging beyond the vasculature with new generation contrast agents. Wiley Interdiscip Rev Nanomed Nanobiotechnol 2015;7 (4):593–608. [PubMed: 25580914]
21. Perera RH, Solorio L, Wu H, Gangolli M, Silverman E, Hernandez C, et al. Nanobubble ultrasound contrast agents for enhanced delivery of thermal sensitizer to tumors undergoing radiofrequency ablation. Pharm Res 2014;31(6):1407–17. [PubMed: 23943542]
22. Wu H, Rognin NG, Krupka TM, Solorio L, Yoshiara H, Guenette G, et al. Acoustic characterization and pharmacokinetic analyses of new nanobubble ultrasound contrast agents. Ultrasound Med Biol 2013;39 (11):2137–46. [PubMed: 23932272]
23. Hernandez C; Abenojar EC; Hadley J; Leon ACD; Coyne R; Perera R; Gopalakrishnan R; Basilion JP; Kolios MC; Exner A. a., sink or float? Characterization of shell-stabilized bulk nanobubbles using a resonant mass measurement technique. Nanoscale11 (3), 2019, 851–855. [PubMed: 30601524]
24. de Leon A, Perera R, Hernandez C, Cooley M, Jung O, Jeganathan S, et al. Contrast enhanced ultrasound imaging by nature-inspired ultrastable echogenic nanobubbles. Nanoscale 2019;11(33):15647–58. [PubMed: 31408083]
25. Maeda H, Nakamura H, Fang J. The EPR effect for macromolecular drug delivery to solid tumors: improvement of tumor uptake, lowering of systemic toxicity, and distinct tumor imaging in vivo. Adv Drug Deliv Rev 2013;65 (1):71–9. [PubMed: 23088862]
26. Shi J, Kantoff PW, Wooster R, Farokhzad OC. Cancer nanomedicine: progress, challenges and opportunities. Nat Rev Cancer 2017;17(1):20–37. [PubMed: 27834398]
27. Kobayashi H, Watanabe R, Choyke PL. Improving conventional enhanced permeability and retention (EPR) effects; what is the appropriate target? Theranostics 2013;4(1):81–9. [PubMed: 24396516]
28. Castanares MA, Mukherjee A, Chowdhury WH, Liu M, Chen Y, Mease RC, et al. Evaluation of prostate-specific membrane antigen as an imaging reporter. J Nucl Med 2014;55(5):805–11. [PubMed: 24700883]
29. Genady AR, Janzen N, Banevicius L, El-Gamal M, El-Zaria ME, Valliant JF. Preparation and evaluation of radiolabeled antibody recruiting small molecules that target prostate-specific membrane antigen for combined radiotherapy and immunotherapy. J Med Chem 2016;59(6):2660–73. [PubMed: 26894427]
30. Barrett JA, Coleman RE, Goldsmith SJ, Vallabhajosula S, Petry NA, Cho S, et al. First-in-man evaluation of 2 high-affinity PSMA-avid small molecules for imaging prostate cancer. J Nucl Med 2013;54(3):380–7. [PubMed: 23303962]
31. Ghosh A, Heston WD. Tumor target prostate specific membrane antigen (PSMA) and its regulation in prostate cancer. J Cell Biochem 2004;91 (3):528–39. [PubMed: 14755683]
32. Sweat SD, Pacelli A, Murphy GP, Bostwick DG. Prostate-specific membrane antigen expression is greatest in prostate adenocarcinoma and lymph node metastases. Urology 1998;52(4):637–40. [PubMed: 9763084]
33. Ristau BT, O'Keefe DS, Bacich DJ. The prostate-specific membrane antigen: lessons and current clinical implications from 20 years of research. Urol Oncol 2014;32(3):272–9. [PubMed: 24321253]
34. Perner S, Hofer MD, Kim R, Shah RB, Li H, Moller P, et al. Prostate-specific membrane antigen expression as a predictor of prostate cancer progression. Hum Pathol 2007;38(5):696–701. [PubMed: 17320151]
35. Kawakami M, Okaneya T, Furihata K, Nishizawa O, Katsuyama T. Detection of prostate cancer cells circulating in peripheral blood by reverse transcription-PCR for hKLK2. Cancer Res 1997;57(19):4167–70. [PubMed: 9331068]

36. Mhawech-Fauceglia P, Zhang S, Terracciano L, Sauter G, Chadhuri A, Herrmann FR, et al. Prostate-specific membrane antigen (PSMA) protein expression in normal and neoplastic tissues and its sensitivity and specificity in prostate adenocarcinoma: an immunohistochemical study using mutiple tumour tissue microarray technique. Histopathology 2007;50(4):472–83. [PubMed: 17448023]
37. Wang X, Huang SS, Heston WD, Guo H, Wang BC, Basilion JP. Development of targeted near-infrared imaging agents for prostate cancer. Mol Cancer Ther 2014;13(11):2595–606. [PubMed: 25239933]
38. Wang X, Tsui B, Ramamurthy G, Zhang P, Meyers J, Kenney ME, et al. Theranostic agents for photodynamic therapy of prostate cancer by targeting prostate-specific membrane antigen. Mol Cancer Ther 2016;15(8):1834–44. [PubMed: 27297866]
39. Abenojar EC, Nittayacharn P, de Leon AC, Perera R, Wang Y, Bederman I, et al. Effect of bubble concentration on the in vitro and in vivo performance of highly stable lipid Shell-stabilized micro- and nanoscale ultrasound contrast agents. Langmuir 2019;35(31):10192–202. [PubMed: 30913884]
40. Lee J, Shen W, Payer K, Burg TP, Manalis SR. Toward attogram mass measurements in solution with suspended nanochannel resonators. Nano Lett 2010;10(7):2537–42. [PubMed: 20527897]
41. Burg TP, Godin M, Knudsen SM, Shen W, Carlson G, Foster JS, et al. Weighing of biomolecules, single cells and single nanoparticles in fluid. Nature 2007;446(7139):1066–9. [PubMed: 17460669]
42. Olcum S, Cermak N, Wasserman SC, Christine KS, Atsumi H, Payer KR, et al. Weighing nanoparticles in solution at the attogram scale. Proc Natl Acad Sci U S A 2014;111(4):1310–5. [PubMed: 24474753]
43. Segers T, Lohse D, Versluis M, Frinking P. Universal equations for the coalescence probability and long-term size stability of phospholipid-coated Monodisperse microbubbles formed by flow focusing. Langmuir 2017;33 (39):10329–39. [PubMed: 28872315]
44. Elias DR, Poloukhtine A, Popik V, Tsourkas A. Effect of ligand density, receptor density, and nanoparticle size on cell targeting. Nanomedicine 2013;9(2):194–201. [PubMed: 22687896]
45. Kuru TH, Tulea C, Simpfendorfer T, Popeneciu V, Roethke M, Hadaschik BA, Hohenfellner M. MRI navigated stereotactic prostate biopsy: fusion of MRI and real-time transrectal ultrasound images for perineal prostate biopsies. Urologe A 2012;51(1):50–6. [PubMed: 21935634]
46. Schouten MG, Hoeks CM, Bomers JG. Hulsbergen-van de Kaa C. a.; Witjes J. a.; Thompson LC; rovers MM; Barentsz JO; Fütterer JJ, location of prostate cancers determined by multiparametric and MRI-guided biopsy in patients with elevated prostate-specific antigen level and at least one negative Transrectal ultrasound–guided biopsy. Am J Roentgenol 2015;205(1):57–63. [PubMed: 26102380]
47. Schoots IG, Roobol MJ, Nieboer D, Bangma CH, Steyerberg EW, Hunink MM. Magnetic resonance imaging–targeted biopsy may enhance the diagnostic accuracy of significant prostate cancer detection compared to standard transrectal ultrasound-guided biopsy: a systematic review and meta-analysis. Eur Urol 2015;68(3):438–50. [PubMed: 25480312]
48. Arsov C, Rabenalt R, Blondin D, Quentin M, Hiester A, Godehardt E, et al. Prospective randomized trial comparing magnetic resonance imaging (MRI)-guided in-bore biopsy to MRI-ultrasound fusion and transrectal ultrasound-guided prostate biopsy in patients with prior negative biopsies. Eur Urol 2015;68(4):713–20. [PubMed: 26116294]
49. Filson CP, Natarajan S, Margolis DJ, Huang J, Lieu P, Dorey FJ, et al. Prostate cancer detection with magnetic resonance-ultrasound fusion biopsy: the role of systematic and targeted biopsies. Cancer 2016;122(6):884–92. [PubMed: 26749141]
50. Siddiqui MM, Rais-Bahrami S, Turkbey B, George AK, Rothwax J, Shakir N, et al. Comparison of MR/ultrasound fusion–guided biopsy with ultrasound-guided biopsy for the diagnosis of prostate cancer. JAMA 2015;313(4):390–7. [PubMed: 25626035]
51. Kaufmann S, Kruck S, Kramer U, Gatidis S, Stenzl A, Roethke M, et al. Direct comparison of targeted MRI-guided biopsy with systematic transrectal ultrasound-guided biopsy in patients with previous negative prostate biopsies. Urol Int 2015;94(3):319–25. [PubMed: 25227711]

52. Afshar-Oromieh A, Haberkorn U, Schlemmer HP, Fenchel M, Eder M, Eisenhut M, et al. Comparison of PET/CT and PET/MRI hybrid systems using a 68Ga-labelled PSMA ligand for the diagnosis of recurrent prostate cancer: initial experience. Eur J Nucl Med Mol Imaging 2014;41(5):887–97. [PubMed: 24352789]

53. Abou-Elkacem L, Bachawal SV, Willmann JK. Ultrasound molecular imaging: moving toward clinical translation. Eur J Radiol 2015;84 (9):1685–93. [PubMed: 25851932]

54. Lee EH, Kim A, Oh YK, Kim CK. Effect of edge activators on the formation and transfection efficiency of ultradeformable liposomes. Biomaterials 2005;26(2):205–10. [PubMed: 15207467]

55. Maeda H, Bharate GY, Daruwalla J. Polymeric drugs for efficient tumor-targeted drug delivery based on EPR-effect. Eur J Pharm Biopharm 2009;71 (3):409–19. [PubMed: 19070661]

56. Hobbs SK, Monsky WL, Yuan F, Roberts WG, Griffith L, Torchilin VP, et al. Regulation of transport pathways in tumor vessels: role of tumor type and microenvironment. Proc Natl Acad Sci U S A 1998;95(8):4607–12. [PubMed: 9539785]

57. Data on file, Lantheus Medical Imaging, Inc.; 2019.

58. Sugimoto K, Moriyasu F, Negishi Y, Hamano N, Oshiro H, Rognin NG, et al. Quantification in molecular ultrasound imaging: a comparative study in mice between healthy liver and a human hepatocellular carcinoma xenograft. J Ultrasound Med 2012;31(12):1909–16. [PubMed: 23197543]

59. Perera R, De Leon AC, Wang X, Ramamurthy G, Peiris P, Basilion J, et al. Nanobubble Extravasation in Prostate Tumors Imaged with Ultrasound: Role of Active Versus Passive Targeting. IUS: EEE Int. Ultrason. Symp; 2018 In press.

60. Chang SS, Reuter VE, Heston WD, Bander NH, Grauer LS, Gaudin PB. Five different anti-prostate-specific membrane antigen (PSMA) antibodies confirm PSMA expression in tumor-associated neovasculature. Cancer Res 1999;59(13):3192–8. [PubMed: 10397265]

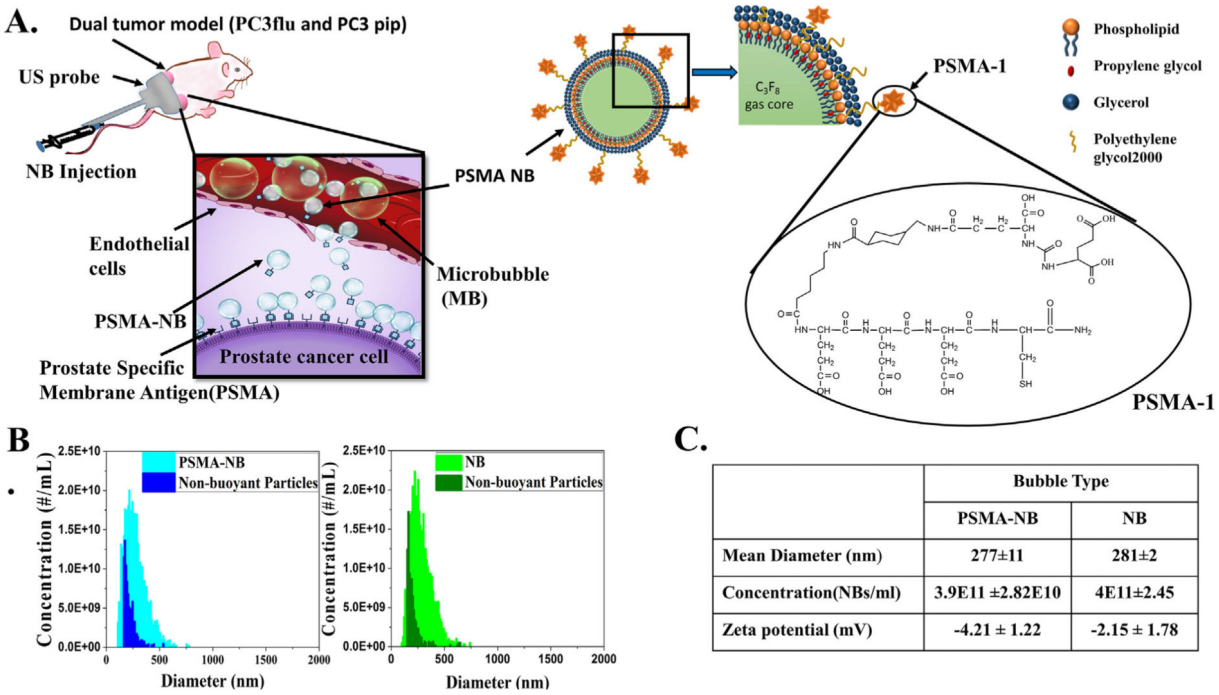

	Bubble Type	
	PSMA-NB	NB
Mean Diameter (nm)	277±11	281±2
Concentration(NBs/ml)	3.9E11 ±2.82E10	4E11±2.45
Zeta potential (mV)	-4.21 ± 1.22	-2.15 ± 1.78

Figure 1.

Design and characterization of PSMA-functionalized NBs for *in vivo* US molecular imaging. (A) Illustration of the experimental setup and schematic illustrating the delivery of PSMA-NB to the tumor parenchyma *via* their leaky vasculature after intravenous injection. DSPE-PEG-PSMA-1 is incorporated into the lipid shell of NB for targeting PCa cells that overexpress PSMA. (B) Size distribution and the concentration of NB and PSMA-NB acquired *via* resonant mass measurement. (C) Size, concentration, and the zeta potential of bubbles. Conjugation of PSMA to the NBs has a minimal effect on the NB properties. Image in panel (a) created by Erika Woodrum.

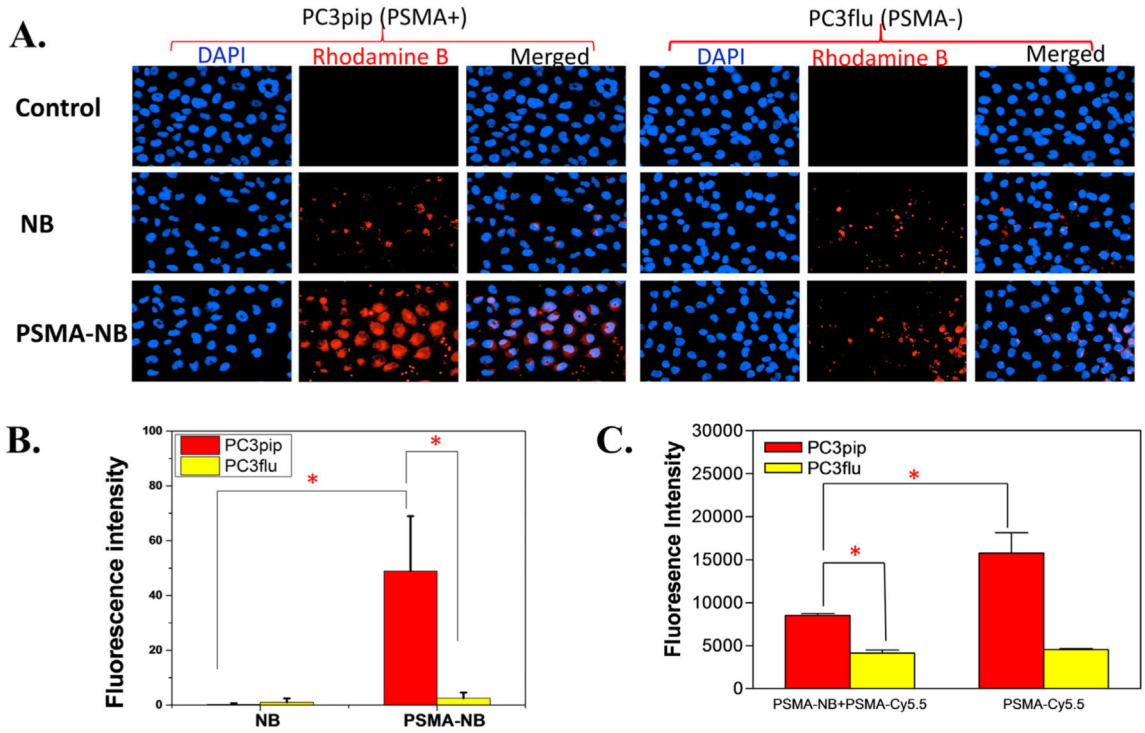

Figure 2.

In vitro cellular uptake experiments reveal PSMA-NB selectively bind to the PSMA-positive PC3pip cells. (A) PC3pip cells and PSMA-negative PC3flu cells on coverslips were incubated with no NB (control), Rhodamine-NB or Rhodamine-PSMA-NB for 1 hr. Nuclei were stained using DAPI (blue) and uptake of Rhodamine tagged bubbles (red) was assessed by fluorescence microscopy (40X). Representative images are shown from three independent experiments. (B) Quantification of fluorescence signal for bubbles with and without 25 μg of PSMA-ligand confirms significant increase in cell specificity with targeted PSMA-NB showing >10-fold increase. (C) Competition experiment of PSMA-NB with PSMA-Cy5.5. Incubation of PSMA-Cy5.5 in the PC3pip cells in the presence of PSMA-NB significantly reduced ($P = 0.0017$) the fluorescence signal compared to the PSMA-Cy5.5 in PC3pip cells. n = 3, error bars represent mean ± s.d., * $P < 0.001$.

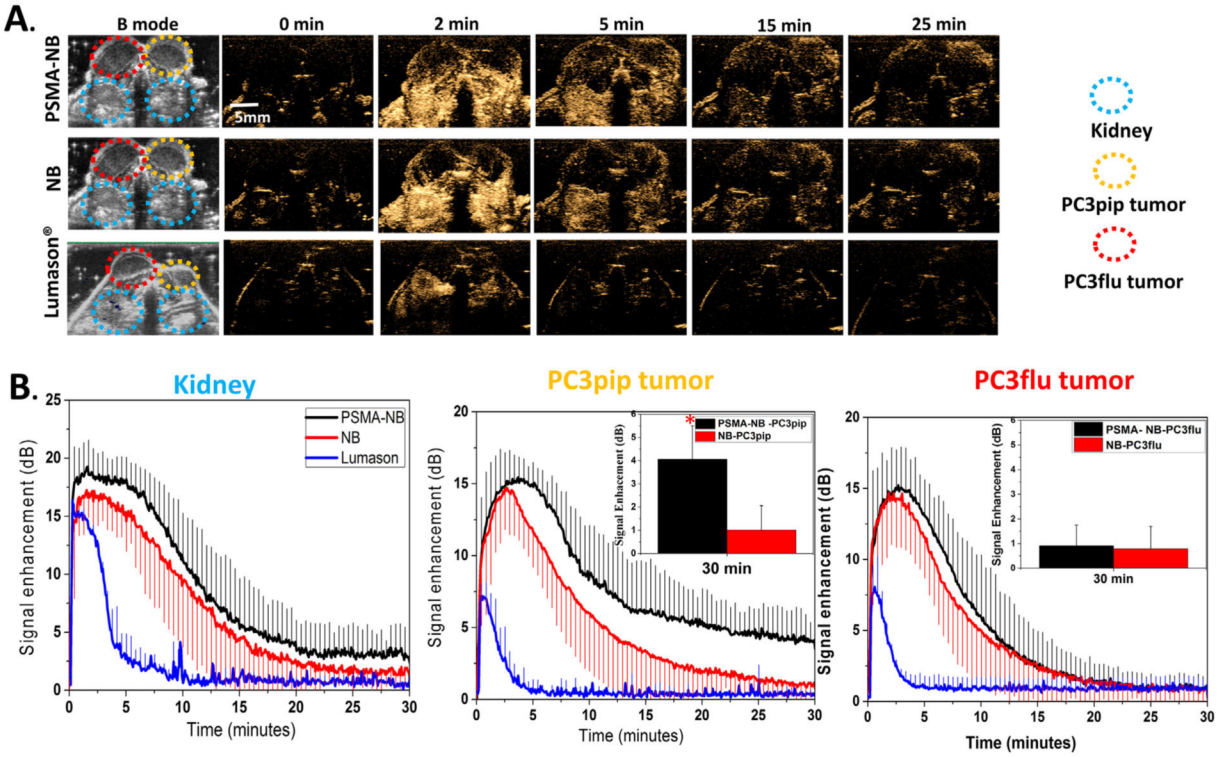

Figure 3.

PSMA-NB enabled imaging of prolonged enhanced US signal in PSMA-positive PC3pip tumors. (A) Representative US imaging results of the targeted PSMA-NB, NB and Lumason® in PC3pip, PC3flu tumors and kidneys. After injection, both tumors and kidneys were imaged at 12 MHz, 0.1MI, and 0.2 frames/second for 30 min. Left two columns show the B-mode and contrast harmonic imaging (CHI) mode images of tumors and kidneys before injection. The series of images shows the CHI images at different time point after bubble administration. At the peak intensity, the contrast in both tumors was similar with both NB and PSMA-NB. At later time points PC3pip tumor show high-contrast with PSMA-NB. (B) Mean time intensity curves (TIC) of tumors, and kidneys after bubble administration. The TIC data was collected from uniform regions of interest drawn on the acquired image stacks. The inset shows the signal intensity of both tumors at 30 min.

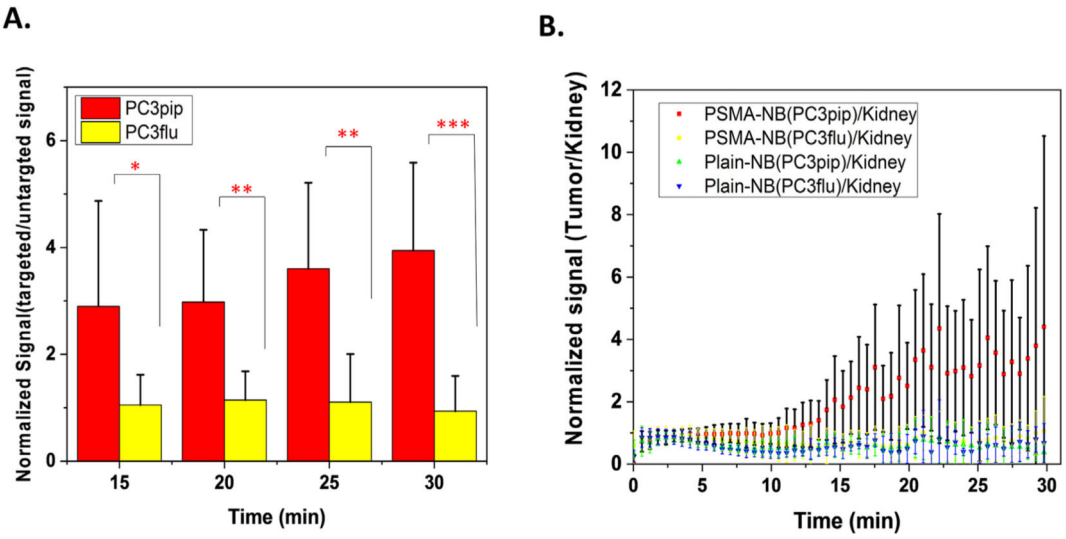

Figure 4.

Normalized signal shows the high ratio with PSMA-NB in PC3pip tumor. (A) US signal obtained from PSMA-NB normalized to the signal from NB at each time point. (B) US signal obtained from PSMA-NB or NB normalized to the same bubble signal in kidney at each time point.

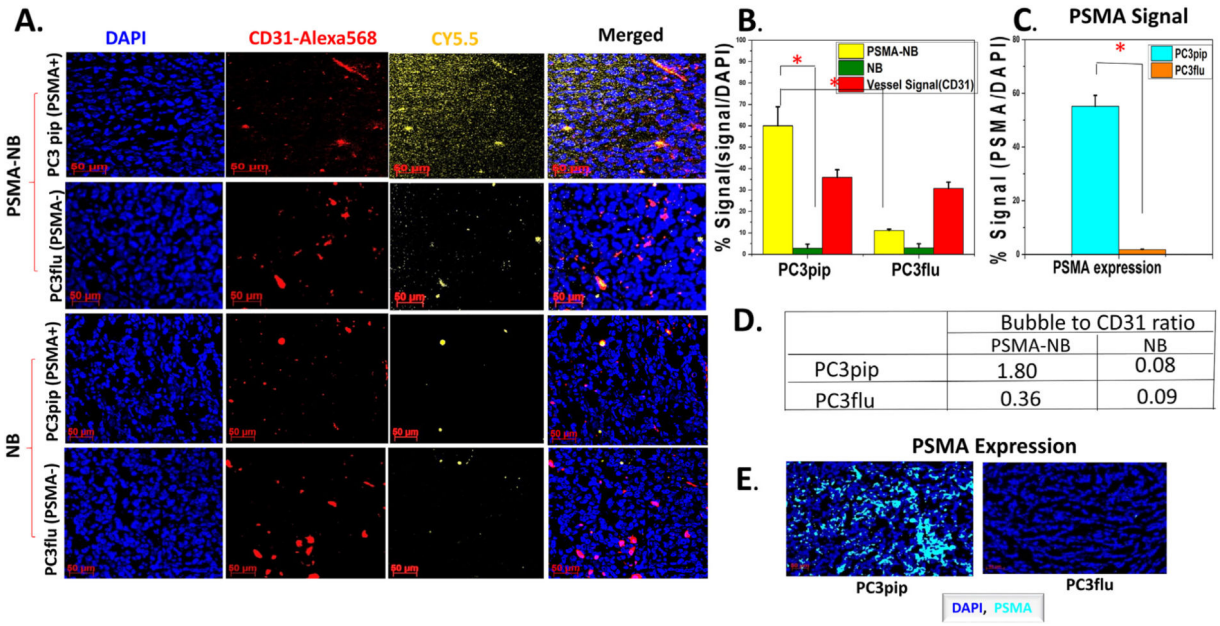

Figure 5.

Histology images confirm the Cy5.5-PSMA-NB accumulation in PSMA-positive PC3pip tumor that were excised after cardiac-perfusion with PBS. (A) Representative fluorescence images showing bubble distribution in tumor(orange). Cy5.5-PSMA-NB showed higher extravasation compared to the Cy5.5-NB. Images show the extravasation of bubbles beyond the tumor vasculature(red). (B) Signal intensities from bubbles and vessels are expressed as the percentage of total cell fluorescence in each tumor section. Cy5.5-PSMA-NB signal in PC3pip tumor is significantly higher from that of PC3flu tumor and the NB signal in PC3pip tumor. (C) PSMA-expression in both tumors as the percentage of total cells of tumor tissues. PSMA-signal in PC3pip tumor is significantly higher than in PC3flu tumor. (D) Bubble to CD31 ratio in both PC3pip and PC3flu tumors. (E) Representative fluorescence images showing higher PSMA-expression in PC3pip tumor compared to that in PC3flu tumor. N = 3, error bars represent mean ± s.d., * $P < 0.001$.

Table 1

Summary of kinetic parameters obtained from time intensity curve (TIC).

Bubble type	Tumor	Peak time (min)	Peak intensity (dB)	Time to reach 25% of peak $-t_{75\%}$(min)	Wash-in AUC	Washout AUC
PSMA-NB	PC3pip	3.95 ± 1.21	15.96 ± 1.83	20.17 ± 8.14 *	49.39 ± 14.54	200.84 ± 31.36 *
	PC3flu	2.75 ± 1.31	15.60 ± 2.53	9.75 ± 3.76	40.32 ± 10.85	112. 06 ± 30.47
NB	PC3pip	2.83 ± 1.90	15.94 ± 2.84	9.71 ± 3.91	39.53 ± 14.33	116.51 ± 25.26
	PC3flu	2.66 ± 1.26	15.05 ± 2.55	8.33 ± 3.03	36.73 ± 13.09	102.17 ± 31.31

N = 7, error bars represent mean ± s.d.

* $P < 0.001$.